

# General Aspects of Entrainment and Deposition in Gravity Mass Flow Models

Dieter Issler

Norwegian Geotechnical Institute, P. O. Box 3930 Ullevål Stadion, N-0806 Oslo, Norway.

Tómas Jóhannesson

Veðurstofa Íslands, Bústaðavegur 7, IS-150 Reykjavík, Iceland.

**Abstract.** Several authors recently proposed adding an “entrainment force” term (equal to minus the entrainment rate times the mean flow velocity) in the momentum balance equations of depth-averaged gravity mass flow models. We show that the entrainment force vanishes if the bed is at rest, but is non-zero in situations where mass is exchanged between adjacent flowing layers or where particles impact on the bed. However, a retarding “entrainment force” must be included if the problem is formulated in terms of an equation of motion.

The entrainment rate  $q_e$  may be limited either by the supply of eroded particles or by their acceleration; in the first case,  $q_e$  grows rapidly with increasing shear stress (or velocity), but decreases with flow velocity in the second case. In the idealized setting of a quasi-stationary, entraining flow of a Bingham fluid, we find a simple relationship between the acceleration of the particles,  $q_e$  and the velocity profile. It allows the velocity and stress profiles to be found in terms of  $q_e$ . The latter can be determined by requiring that the bed shear stress be equal to the erosion threshold of the bed material. This boundary condition is expected to be approximately valid for a wide class of materials.

For continuous deposition to occur, the bed shear stress must exceed the maximum shear stress inside the flowing material, and stopped flow particles must sinter to the bed very rapidly. The deposition rate is limited by the difference between internal and bed shear stresses and by the inverse of the flow velocity.

snow avalanches and pyroclastic flows. In particular, field studies of snow avalanches (Issler et al., 1996; Sovilla et al., 2001) revealed that the moving mass may increase by an order of magnitude over the mass released initially. However, detailed experimental information on the mechanisms leading to the loosening of bed particles and their eventual mixing into the flow is scarce. Interesting studies of granular flows (Barbolini et al., 2005) and snow avalanches (Sovilla, 2004) have recently begun to shed some light on these questions. In the field of fluvial hydraulics, a number of experiments in circular flumes have established empirical relations between the bottom shear stress, the strength of the bed material and the entrainment rate. A few among the numerous studies of drifting sand and snow have measured the spatial rate of approach to saturated flow (Takeuchi, 1980) or investigated the rebounding of impacting particles and the ejection of bed particles (White, 1982; Rice et al., 1996).

Snow avalanches were among the first gravity mass flows for which dynamical models were developed. Already at an early stage, models including either entrainment at the front or along the bottom of the flow were proposed in Russia. Entrainment was described in analogy either with shocks in gas dynamics (Briukhanov et al., 1967; Grigorian and Ostroumov, 1977) or with the theory of mixing at the interface in a stratified flow (Eglit, 1983). Unfortunately, this pioneering work was largely unknown or ignored outside Russia. In the 1980s and 1990s, models of turbidity currents (Parker et al., 1986) and powder snow avalanches (Fukushima and Parker, 1990; Hermann et al., 1994; Issler, 1998; Naaim and Gurer, 1998) with different entrainment mechanisms were proposed and used with some success. In recent years, the mentioned experimental work has motivated new attempts at modeling entrainment in dense-flow avalanches. The applied concepts range from a fixed entrainment depth (Sovilla and Bartelt, 2002) over a modified Grigorian–Ostroumov model (Sovilla, 2004) and an interesting heuristic “bottom and top” mechanism (Sailer et al., 2002) to a detailed consid-

---

## 1 Introduction

Entrainment of ambient fluid or bed material has long been recognized as an important process in many types of gravity mass movements such as debris flows, turbidity currents,

---

*Correspondence to:* Dieter Issler (di@ngi.no)

eration of stresses (Naaim et al., 2004). Eglit and Demidov (2005) compared and tested a variety of empirical entrainment mechanisms and parameterizations proposed in different areas of application. They found no pronounced differences between the different entrainment laws, but this may be largely due to the rather small mobilizable mass they assumed.

All models based on the shallow-water approximation agree on the general form of the mass balance equation, here written for the one-dimensional case and for constant flow density  $\rho_f$  (which may differ from the bed density  $\rho_b$ ):

$$\partial_t h + \partial_x(h\bar{u}) = q/\rho_f. \quad (1)$$

$t$  and  $x$  are the time and the distance along the path,  $h$  is the flow depth,  $u$  the velocity, and  $q$  the mass entrainment rate. Overlining denotes depth-averaged quantities. The depth of the bed,  $b(x, t)$ , evolves according to

$$\partial_t b = -q/\rho_b. \quad (2)$$

There is long-standing disagreement (Cannon and Savage, 1988; Hungr, 1990; Cannon and Savage, 1990; Erlichson, 1991) over the correct form of the momentum balance equation. Some of the early as well as of the more recent papers (but none of the mentioned Russian works) supplement the momentum balance in its customary form with a decelerating “entrainment force” term  $-q\bar{u}$  (Sovilla and Bartelt, 2002; Naaim et al., 2004)<sup>1</sup>:

$$\begin{aligned} & \partial_t(h\bar{u}) + \partial_x(h\bar{u}^2) \\ &= hg \sin \theta + \frac{1}{\rho_f} \partial_x(h\bar{\sigma}_{xx}) - \frac{\sigma_{xz}^{(b)}}{\rho_f} - \frac{q}{\rho_f} \bar{u}. \end{aligned} \quad (3)$$

In (3),  $g$  is the gravitational acceleration,  $\theta(x)$  the local slope angle,  $\bar{\sigma}_{xx}$  the depth-averaged longitudinal normal stress (the negative of the “earth pressure”), and  $\sigma_{xz}^{(b)}$  the shear stress at the interface to the bed, indicated by the superscript  $(b)$ . A closely related issue is the treatment of momentum loss during deposition. There is also disagreement as to how the bed shear strength  $\tau_c$  (the minimum shear stress required to break the bonds between the bed particles) relates to the bed shear stress obtained from the rheological assumptions. These questions have significant practical impact: At the instrumented test site for snow avalanches at Vallée de la Sionne in the Swiss Alps, bed erosion rates exceeding  $100 \text{ kg m}^{-2} \text{ s}^{-1}$  at a flow velocity of about  $50 \text{ m s}^{-1}$  have been measured (Gauer and Issler, 2004); if the “entrainment force” exists,

it amounts to  $-5 \text{ kPa}$  in this case and clearly dominates the force balance of the avalanche.

The purpose of this paper is to propose a consistent continuum mechanical framework in which to study all these questions. Some of the answers given here are not new, but they are scattered in the literature or have not been explicitly discussed. It will be seen that a precise definition of the mechanical system to be described (Sect. 2) is the key to determining under which conditions an “entrainment force” needs to be introduced (Sect. 3). If this system definition is supplemented by qualitative micromechanical considerations, it becomes clear how to account for the resistance of the bed material. The distinction between erosion (the breaking of the inter-particle bonds in the bed material) and entrainment (the process of mixing the loose particles into the flow) stressed by Gauer and Issler (2004) then naturally links the erosion threshold stress and the mixing process to the shear rate at the interface to the bed; this will be detailed in Sect. 4. Deposition is in many respects the reverse process of entrainment, but Sect. 5 will show that additional conditions related to solidification and internal and bed shear stresses must be fulfilled.

## 2 Basic notions

When a fluid or particulate flow runs over an erodible bed, the shear stress it exerts on the particles constituting the bed may exceed the strength of the bed material. This may occur either locally during short time intervals because of turbulent eddies or particle impacts, or quasi-continuously over large areas in laminar fluid flows or dense particulate flows. Under such conditions, bonds between bed particles are broken and single particles or larger chunks of material become loose. The breaking of the bonds is a rapid process (treated as instantaneous here) that will be called *erosion* in this paper, following the terminology of Gauer and Issler (2004). Once broken loose, the bed material will be accelerated by the flow and often mixed into it. This phase is termed *entrainment*.

The time when a particle or chunk of material leaves the bed and becomes part of the flow is a matter of definition, but it appears most natural to consider a particle as part of the bed as long as it is at its original location. The interface between the flow and the bed is thus the boundary of the area where  $\mathbf{u} \neq \mathbf{0}$  in the rest frame of the bed<sup>2</sup>. An immediate consequence—central to the controversy on entrainment forces in the equations of motion—is that the velocity of ma-

<sup>1</sup>There is some inconsistency in the formulation of the momentum balance equation between different papers and reports by these (and other) authors. The “entrainment force” term is absent in the momentum balance equation in (Sovilla, 2004) and is not included in the computational code of the MN2L snow avalanche model to account for the acceleration of eroded bed particles (M. Naaim, personal communication, 2005).

<sup>2</sup>Note, however, that high-speed videos of granular flows over granular beds (M. Barbolini and M. Pagliardi, personal communication, 2005) or of cohesive debris over a similar bed (H. Breien and M. Pagliardi, personal communication, 2006) show that the bed may be set into slow shearing motion before erosion and entrainment occur or even if entrainment does not occur at all. In this case,  $\mathbf{u}^{(b)} \neq \mathbf{0}$  at the interface, but still  $\mathbf{u}^{(b)} \ll \bar{\mathbf{u}}$ .

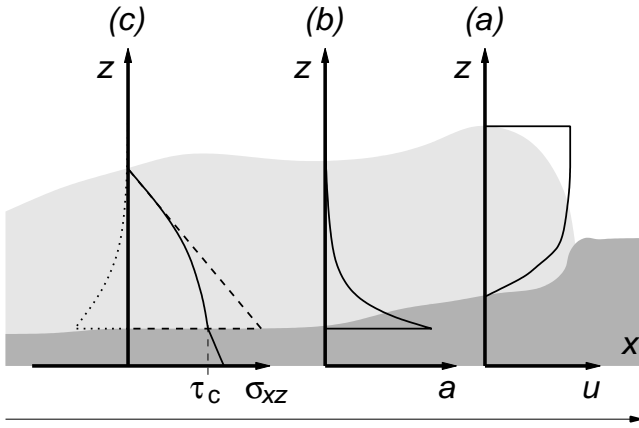


**Fig. 1.** Schematic representation of a gravity mass flow over an erodible bed. The interface shown is that between bed particles at rest and flow or bed particles in motion. (a) Qualitative velocity profile. (b) Qualitative acceleration profile. Note that a quasi-stationary flow is assumed so that acceleration is confined to the mixing region near the interface. (c) Qualitative shear stress profile, showing the (integrated) contributions due to the weight of the flowing material (dashed line) and the inertial pseudo-force due to the acceleration of the eroded bed material (dotted line). The resulting net shear stress (full line) tends to the threshold value  $\tau_c$  at the erosion interface.

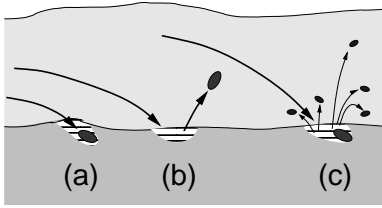


**Fig. 2.** Schematic representation of the mass and momentum exchange processes between an erodible bed and a layer of saltating particles. Impacting particles may be absorbed by the bed (a) or rebound (b), and bed particles may be ejected with non-zero initial velocity as a result of the impact (c).

material at the transition from bed to flow and vice versa is zero (see Fig. 1).

However, that conclusion does not hold true in sand and snow drift: Particles in the saltation layer impact on the bed at velocities close to the mean flow velocity and may be absorbed by the bed or may rebound from it with another speed and direction (Fig. 2). The impact may also cause bed particles to be ejected with non-zero initial velocities. The mass exchange across the interface is in such cases accompanied by a net momentum flow carried by the particles. In the literature, the so-called grain-borne shear stress is therefore distinguished from the shear stress exerted by the ambient fluid. Examples of the resulting momentum balance equations can be found in (Issler, 1998; Issler et al., 2000; Gauer, 2001).

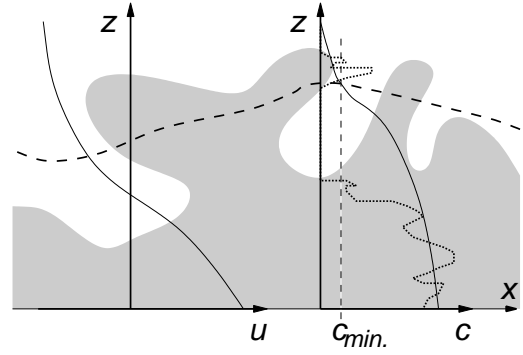


**Fig. 3.** Schematic representation of the upper interface of a turbidity current, a pyroclastic flow or a powder snow avalanche. The instantaneous and time-averaged concentration profile (right profile, dotted and full lines) and time-averaged velocity profile (left profile) are indicated. The interface shown is the instantaneous boundary of the area with particles. The thick dashed line indicates the boundary where the time-averaged concentration  $\bar{c}$  drops below  $\bar{c}_{min}$ .

In other types of stratified flow with mass exchange, criteria adapted to the situation need to be specified to define the layer boundaries in an unambiguous way. A common and important case is the upper boundary of the suspension layer in turbidity currents, powder snow avalanches and pyroclastic flows, discussed in some detail by Issler et al. (2000): Particle concentration diminishes to very low values at the upper boundary of the layer, which is nevertheless clearly visible. One might thus try to define the layer boundary as the (instantaneous) surface above which the particle concentration is zero. This definition requires some refinement, however, because of the irregular and rapidly fluctuating nature of interfaces in highly turbulent flows. Choosing a time scale that is short compared to the overall evolution of the flow but long on the scale of turbulent eddies, one may set the boundary at the surface where the time-averaged concentration exceeds some low threshold value, see Fig. 3. The velocity is continuous across that surface, but in general non-zero. Entrainment of ambient fluid into the flow therefore not only adds mass to the flow but also momentum. In many types of stratified flows such as turbidity currents and powder snow avalanches, the ambient fluid displaced by the front flows over and opposite to the particle flow. The interface is therefore a region of intense shear but low velocities so that the momentum flow due to the mass exchange often plays a secondary role.

Inside a non-entraining, stationary and spatially uniform gravity mass flow, the shear stress is balanced by gravity. The momentum balance in the flow direction ( $x$ ) thus reduces to  $\partial_z \sigma_{xz} + \rho g \sin \theta$  or, equivalently,  $\sigma_{xz}(z) = \rho g(h - z) \sin \theta$ , where  $z$  is the bed-normal coordinate. However, if bed material is entrained into the flow, the eroded particles must be accelerated by a net force acting on them. Even if the main flow is quasi-stationary, the region close to the interface is not when there is entrainment. The momentum bal-

ance then yields  $\sigma_{xz}(z) = \rho g(h-z) \sin \theta - \int_z^h \rho D_t u_x dz' < \rho g(h-z) \sin \theta$  since the material derivative  $D_t u_x = \partial_t u_x + \mathbf{u} \cdot \nabla u_x > 0$  in the bottom layer; see the schematic shear stress profiles in Fig. 1. We will argue in Sect. 4 that the value of  $\sigma_{xz}^{(b)}$  should be very close to the erosion threshold stress  $\tau_c$ .

The acceleration of mass is a continuous process. If the flowing and bed material were continuous media in the mathematical sense, entrainment would preclude a slip velocity at the bed–flow interface. However, this is not valid in flows with particle ejection triggered by impacts or in particulate flows with moderate erosion rates: The flow may slide over the bed, only now and then breaking a bed particle loose and entraining it.

### 3 Modifications of the balance equations for mass and momentum

In order to deduce the correct form of the depth-averaged momentum balance for a flow with entrainment, consider first the full two- or three-dimensional formulation of the flow of a granular, cohesionless material over a bed of similar particles. The mechanical system that is being described comprises both the flowing material and the bed. If the shear stress exceeds the shear strength  $\tau_y = \sigma_n \tan \phi$  of the bed material (characterized by its internal friction angle  $\phi$  and the normal stress  $\sigma_n$ ), a portion of the latter will be set in motion. In this description, entrainment is merely seen as the beginning of motion of a material element inside the domain. All of this is described by the usual balance equations and the constitutive equation of the material, which must be formulated in such a way as to cover the solid–fluid transition. There is neither a mass source term in the mass conservation equation nor a specific entrainment term in the momentum balance equations.

It may, however, be desirable for practical reasons to describe only the flowing material and to specify bed entrainment or deposition by means of mass and momentum fluxes through the system boundary. (This is the approach chosen in the mentioned papers on powder snow avalanches.) The flow is divided into slices of infinitesimal length  $\Delta x$  that extend over the entire depth of the flow (Fig. 4.a). In the Euler representation, the boundaries 1 and 3 are fixed, i. e., their velocities  $\mathbf{w}_{1,3} = \mathbf{0}$ . The boundaries 2 and 4 are moving with velocities

$$\mathbf{w}_2(x, t) = \hat{\mathbf{k}} \partial_t b(x, t), \quad \mathbf{w}_4(x, t) = \hat{\mathbf{k}} \partial_t s(x, t) \quad (4)$$

expressed in terms of the functions  $b(x, t)$  and  $s(x, t)$  describing the location of the interfaces. The orthonormal basis vectors  $\hat{\mathbf{i}}, \hat{\mathbf{k}}$  are parallel and normal to the bottom of the

erodible bed, respectively<sup>3</sup>. The conservation equations for mass and momentum, integrated over the slice, are

$$\frac{d}{dt} \int_V dV \rho + \oint_{\partial V} dA \rho (\mathbf{u} - \mathbf{w}) \cdot \hat{\mathbf{n}} = 0, \quad (5)$$

$$\begin{aligned} \frac{d}{dt} \int_V dV \rho \mathbf{u} + \oint_{\partial V} dA \rho \mathbf{u} (\mathbf{u} - \mathbf{w}) \cdot \hat{\mathbf{n}} \\ = \int_V dV \rho \mathbf{g} + \oint_{\partial V} dA \boldsymbol{\sigma} \cdot \hat{\mathbf{n}}. \end{aligned} \quad (6)$$

The volume integrals are evaluated straightforwardly in terms of the flow depth  $h(x, t) = s(x, t) - b(x, t)$  and the depth-averaged quantities  $\bar{\rho}, \bar{\mathbf{u}}$ :<sup>4</sup>

$$\frac{d}{dt} \int_V dV \rho(x, z, t) = \partial_t (h(x, t) \bar{\rho}(x, t)) \Delta x, \quad (7)$$

$$\begin{aligned} \frac{d}{dt} \int_V dV \rho(x, z, t) \mathbf{u}(x, z, t) \\ = \partial_t (h(x, t) \bar{\rho}(x, t) \bar{\mathbf{u}}(x, t)) \Delta x, \end{aligned} \quad (8)$$

$$\int_V dV \rho(x, z, t) \mathbf{g} = h(x, t) \bar{\rho}(x, t) \mathbf{g} \Delta x. \quad (9)$$

The space and time dependence of the variables is explicitly shown here, but will be suppressed henceforth where no confusion is possible.

It is convenient to evaluate the surface integrals separately for each side. The contributions to the advective terms from sides 1 and 3 combine to

$$\begin{aligned} \int_{b+\Delta b}^{s+\Delta s} dz \rho(x + \Delta x, z, t) u_x(x + \Delta x, z, t) \\ - \int_b^s dz \rho(x, z, t) u_x(x, z, t) \\ \longrightarrow \partial_x \int_b^s dz \rho u_x \Delta x = \partial_x (h \bar{\rho} \bar{u}_x) \Delta x \end{aligned} \quad (10)$$

and

$$\partial_x \int_b^s dz u_x \rho \mathbf{u} \Delta x = \partial_x (h \bar{\rho} \bar{u}_x \bar{\mathbf{u}}) \Delta x \quad (11)$$

as  $\Delta x \rightarrow 0$ . Similarly one obtains

$$\begin{aligned} \int_{\partial V_1 \cup \partial V_3} dA \boldsymbol{\sigma} \cdot \hat{\mathbf{n}} \longrightarrow \partial_x \int_b^s dz \boldsymbol{\sigma} \cdot \hat{\mathbf{i}} \Delta x \\ = \partial_x (h \bar{\boldsymbol{\sigma}}) \cdot \hat{\mathbf{i}} \Delta x \end{aligned} \quad (12)$$

<sup>3</sup>The basis vectors  $\hat{\mathbf{i}}$  and  $\hat{\mathbf{k}}$  point in the local  $x$  and  $z$  directions, which are defined as tangent and normal to the slope. If the slope angle is variable, additional terms related to the curvature arise, but we disregard this complication here. For a treatment of these geometrical effects see e. g. (Eglit, 1983; Savage and Hutter, 1991; Gray et al., 1999).

<sup>4</sup>If the density is variable, Favre averaging is used for the velocity so that  $\bar{\rho} \bar{\mathbf{u}} = \bar{\rho} \bar{\mathbf{u}}$  by definition.

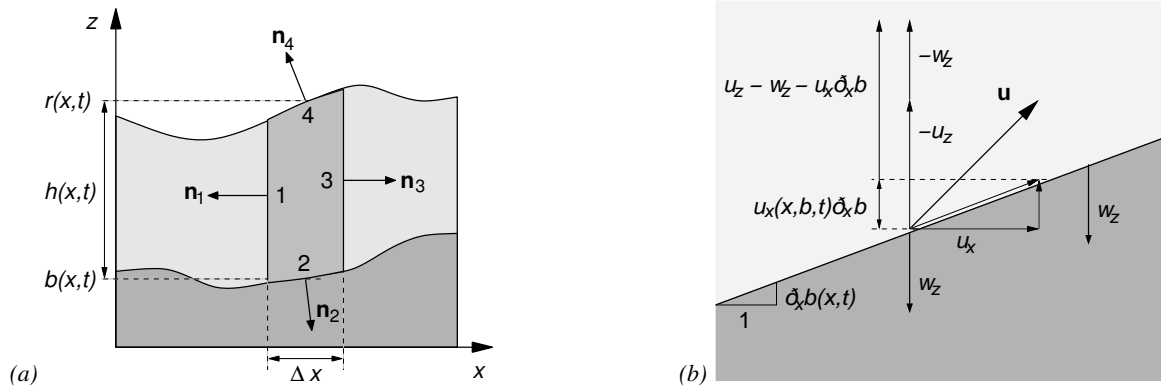


**Fig. 4.** (a) Definition sketch of the integration volume used in the derivation of the mass and momentum balance equations in the presence of bed entrainment (or deposition to the bed). (b) Schematic representation of the mass flux through a moving inclined boundary.

for the stress integral over the sides 1 and 3.

When evaluating the integrals on the sides 2 and 4, possible density and velocity discontinuities have to be taken into account by using the jump conditions

$$\begin{aligned} \llbracket \rho(\mathbf{u} - \mathbf{w}) \cdot \hat{\mathbf{n}} \rrbracket &:= \rho(\mathbf{r}^+, t)[\mathbf{u}(\mathbf{r}^+, t) - \mathbf{w}(\mathbf{r}, t)] \cdot \hat{\mathbf{n}} \\ &\quad - \rho(\mathbf{r}^-, t)[\mathbf{u}(\mathbf{r}^-, t) - \mathbf{w}(\mathbf{r}, t)] \cdot \hat{\mathbf{n}} \\ &= 0, \end{aligned} \quad (13)$$

$$\llbracket \rho \mathbf{u}(\mathbf{u} - \mathbf{w}) \cdot \hat{\mathbf{n}} \rrbracket = \llbracket \boldsymbol{\sigma} \cdot \hat{\mathbf{n}} \rrbracket. \quad (14)$$

The length of the boundary lines is  $\Delta x \sqrt{1 + (\partial_x b)^2}$  and  $\Delta x \sqrt{1 + (\partial_x s)^2}$ , respectively. The unit normal vectors can be expressed as

$$\begin{aligned} \hat{\mathbf{n}}_2 &= \frac{1}{\sqrt{1 + (\partial_x b)^2}} \begin{pmatrix} \partial_x b \\ -1 \end{pmatrix}, \\ \hat{\mathbf{n}}_4 &= \frac{1}{\sqrt{1 + (\partial_x s)^2}} \begin{pmatrix} -\partial_x s \\ 1 \end{pmatrix}, \end{aligned} \quad (15)$$

the boundary velocities are given by (4). In the bed, the material is at rest. Suppressing the dependence of the fields on  $x$  and  $t$  and indicating the  $z$ -dependence with superscripts  $(b)$  and  $(s)$ , respectively, we obtain the kinematic boundary condition (KBC) at the bottom surface from Eq. (13)<sup>5</sup>:

$$\rho^{(b^+)} \left[ \partial_t b + u_x^{(b^+)} \partial_x b - u_z^{(b^+)} \right] = \rho^{(b^-)} \partial_t b \equiv -q_b. \quad (16)$$

At the upper surface an analogous KBC is obtained, but the velocity of the ambient fluid is not zero in general:

$$\begin{aligned} \rho^{(s^-)} \left[ \partial_t s + u_x^{(s^-)} \partial_x s - u_z^{(s^-)} \right] \\ = \rho^{(s^+)} \left[ \partial_t s + u_x^{(s^+)} \partial_x s - u_z^{(s^+)} \right] \equiv -q_s. \end{aligned} \quad (17)$$

<sup>5</sup>Note that we define the entrainment rate as the mass flux perpendicular to the local  $x$ -direction and not perpendicular to the interface.

If the upper surface is material, i.e., no mass is passing through it, the suspension rate is zero and one obtains the KBC in its usual form,  $\partial_t s + u_x^{(s^-)} \partial_x s - u_z^{(s^-)} = 0$ . Similar relations are obtained from the momentum jump condition (14) if use is made of (16) and (17):

$$\begin{aligned} (u_x^{(b^+)} - u_x^{(b^-)}) q_b \\ = \sigma_{xz}^{(b^+)} - \sigma_{xz}^{(b^-)} - (\sigma_{xx}^{(b^+)} - \sigma_{xx}^{(b^-)}) \partial_x b, \end{aligned} \quad (18)$$

$$\begin{aligned} (u_x^{(s^+)} - u_x^{(s^-)}) q_s \\ = \sigma_{xz}^{(s^+)} - \sigma_{xz}^{(s^-)} - (\sigma_{xx}^{(s^+)} - \sigma_{xx}^{(s^-)}) \partial_x s. \end{aligned} \quad (19)$$

If  $q_b$  and  $q_s$  are zero or the velocity is continuous at the interfaces, the shear stresses parallel to the interfaces are continuous. The  $z$ -component of the momentum jump condition at the bed,

$$\begin{aligned} (u_z^{(b^+)} - u_z^{(b^-)}) q_b \\ = \sigma_{zz}^{(b^+)} - \sigma_{zz}^{(b^-)} - (\sigma_{zx}^{(b^+)} - \sigma_{zx}^{(b^-)}) \partial_x b, \end{aligned} \quad (20)$$

is not needed if hydrostatic pressure distribution is assumed.

With the help of (16)–(19), the mass and momentum fluxes across the boundaries 2 and 4 can be evaluated easily. Combining (7) and (10) with (16) and (17), we obtain

$$\partial_t (h\bar{\rho}) + \partial_x (h\bar{\rho} \bar{u}_x) = q_b - q_s \equiv q_e, \quad (21)$$

as expected, with  $q_e$  the total entrainment rate. For the momentum balance we use (8), (9), (11), (18) and (19):

$$\begin{aligned} \partial_t (h\bar{\rho} \bar{u}_x) + \partial_x \left( h\bar{\rho} \bar{u}_x^2 \right) \\ = h\bar{\rho} g \sin \theta + \partial_x (h\bar{\sigma}_{xx}) + \sigma_{xz}^{(s^+)} - \sigma_{xz}^{(s^-)} \partial_x s \\ - \sigma_{xz}^{(b^-)} + \sigma_{xx}^{(b^-)} \partial_x b - q_s u_x^{(s^+)} + q_b u_x^{(b^-)} \end{aligned} \quad (22)$$

Expression (22) differs from those given in (Sovilla and Bartelt, 2002; Naaim et al., 2004) with respect to the sign of

the entrainment term and the precise meaning of the velocity in it: The velocity is to be evaluated at the interface and thus is to be set to zero in the situation considered by those authors. As shown in detail by Issler et al. (2000), (22) is compatible with the entrainment terms in the two-layer model proposed in (Issler, 1998). The front-entrainment model in (Briukhanov et al., 1967) and the base-entrainment model by Grigorian and Ostroumov (1977) directly use the jump conditions and are formulated correctly. The two-layer model by Eglit and co-workers summarized in (Eglit, 1998) assumes  $\mathbf{u} = \mathbf{0}$  at the bed-avalanche interface and is devoid of spurious “entrainment force” terms; it also correctly describes the particle-borne momentum flux between the dense-flow and powder-snow layers.

It is instructive to convert the momentum-balance (22) into the equivalent equation of motion by substituting the mass balance (21) into it, assuming  $\rho = \text{const.}$  in the flow and no shear stress at the upper surface. Using the advective derivative  $D_t \equiv \partial_t + \bar{u}_x \partial_x$ , the result is

$$\begin{aligned} D_t \bar{u}_x = g \sin \theta + \frac{1}{h\bar{\rho}} \left[ \partial_x (h\bar{\sigma}_{xx}) - \sigma_{xz}^{(b)} + \sigma_{xx}^{(b)} \partial_x b \right] \\ - \frac{1}{h\bar{\rho}} \partial_x \left[ h\bar{\rho} \left( \bar{u}_x^2 - \bar{u}_x'^2 \right) \right] \\ - \frac{1}{h\bar{\rho}} \left( q_e \bar{u}_x + q_s u_x^{(s+)} - q_b u_x^{(b-)} \right). \end{aligned} \quad (23)$$

The next-to-last term would vanish if the velocity profile were uniform, and is small in most cases. This equation of motion indeed features an entrainment pseudo-force (the last term), which is equivalent to a retarding stress  $-q_e \bar{u}_x$  in case of entrainment ( $q_e > 0$ ) if the interface velocities are zero, as is often the case in a single-layer model. It may be interpreted in the following way: A small volume that is moving in the flow at time  $t$  experiences a decelerating force due to the mixing with the mass that is entrained between  $t$  and  $t + \Delta t$  and is being accelerated in the process. The mixing redistributes momentum from the fast-moving mass in the flow to the freshly entrained, slow mass. It may be noted that the effect of entrainment on the momentum balance of the flow in Eq. (23) is identical to the effect of entrained water from the melting of ice from englacial tunnel walls on the momentum balance of sudden outburst floods from glaciers, which are called jökulhlaups (Spring and Hutter, 1981, Eq. (2.2)).

#### 4 Relation between the entrainment rate and the velocity profile in quasi-steady flow

The equation of motion (23) suggests at first sight that strong entrainment might decelerate and eventually stop a gravity mass flow due to the last term, which is proportional to the entrainment rate. Conversely, if deposition is sufficiently rapid ( $q \ll 0$ ), could it be that the last term overwhelms the retarding terms and accelerates the flow? Such behaviour is

counter-intuitive and even violates the Second Law of thermodynamics because entrainment and deposition are consequences of dissipative forces that oppose relative motion. What Eq. (23) hides is the subtle interplay between the shear stresses and the entrainment or deposition rate.

Consider a hypothetical material that behaves as a solid with a shear strength  $\tau_c$ , above which it disintegrates into a cohesive granular fluid with a yield strength  $\tau_y < \tau_c$  and (Bingham) kinematic viscosity  $\nu$ :

$$\dot{\gamma}(z) = \partial_z u_x = \begin{cases} 0, & |\sigma_{xz}| \leq \tau_y; \\ \text{sgn}(\sigma_{xz}) \frac{|\sigma_{xz}| - \tau_y}{\rho_f \nu}, & |\sigma_{xz}| \geq \tau_y. \end{cases} \quad (24)$$

In order to concentrate on the essential points and obtain analytic solutions, we consider an infinitely extended slope with inclination  $\theta$ , on which an infinitely long sheet of depth  $h$  (measured perpendicular to the slope) flows at constant speed. This assumption eliminates the gradient of the longitudinal stresses. We further suppose that the eroded bed material is immediately replenished from below so that the interface between bed and flow is inclined at the same angle  $\theta$ , and that material is taken away from the top of the flow (without application of shear stresses) at the same rate as it is entrained from below so that the total flow depth and the plug-layer depth remain constant. Under these conditions, a steady flow is possible and the flowing material has a constant velocity component  $w_e = u_x = q/\rho_f$  normal to the bed; momentum is taken away from the system at the rate  $-\rho_f u_x (h) w_e$ .

The plug-layer extends from the surface of the flow to a height  $r$  above the bed:

$$r = h - \frac{\tau_y}{\rho_f g \sin \theta}. \quad (25)$$

In the absence of entrainment, the shear stress profile would be linear,

$$\sigma_{xz}^{(0)}(z) = \rho_f g (h - z) \sin \theta, \quad (26)$$

the shear rate would diminish linearly from the bed to the height  $r$ ,

$$\dot{\gamma}^{(0)}(z) = \begin{cases} \frac{g(r-z) \sin \theta}{\nu}, & z \leq r; \\ 0, & z \geq r, \end{cases} \quad (27)$$

and the velocity profile would be parabolic in the shear layer if there is no sliding at the bed,

$$u_x^{(0)}(z) = \begin{cases} \frac{g \sin \theta}{2\nu} (2rz - z^2), & z \leq r; \\ \frac{g \sin \theta}{2\nu} r^2, & z \geq r. \end{cases} \quad (28)$$

With entrainment in our idealized situation, the velocity profile will remain constant in time, but deviate from Eq. (28).

The mass balance equation is trivially satisfied with bed entrainment balanced by the mass removal at the top surface and  $h = \text{const.}$  In order to solve the equation of motion (or, alternatively, the momentum balance equation), we

need a relation between the acceleration of a flow particle and the erosion speed  $w_e$ . Over a short time interval  $\Delta t$ , a flow particle moves from its vertical position at  $z$  to  $z + \Delta z = z + w_e \Delta t$ ; thereby, its longitudinal velocity component changes by  $\Delta u_x = u_x(z + \Delta z) - u_x(z) = \dot{\gamma}(z) \Delta z$ . Hence the acceleration is

$$\frac{du_x}{dt} = w_e \dot{\gamma}(z). \quad (29)$$

This result does not depend on the particular rheology we have assumed and is generally valid if the flow is stationary.

The equation of motion for a fluid element may now be formulated as

$$\frac{du_x}{dt}(z, t) = w_e \dot{\gamma}(z) = g \sin \theta + \frac{1}{\rho_f} \frac{d\sigma_{xz}}{dz}(z). \quad (30)$$

In a stationary flow without entrainment, the right-hand side of this equation would be zero, allowing evaluation of the profiles of the shear stress and—by means of the constitutive equation—of the shear rate and the velocity, as in Eqs. (26)–(28). With entrainment, however, the constitutive equation is used to transform Eq. (30) into a differential equation for the shear rate, with the entrainment speed treated as an external parameter:

$$\frac{d\dot{\gamma}}{dz}(z) - \frac{w_e}{\nu} \dot{\gamma}(z) = -\frac{g \sin \theta}{\nu}. \quad (31)$$

The boundary condition  $\dot{\gamma}(r) = 0$  leads to the solution

$$\dot{\gamma}(z) = \begin{cases} \frac{g \sin \theta}{w_e} \left( 1 - e^{-\frac{w_e}{\nu}(r-z)} \right), & 0 \leq z \leq r; \\ 0 & r \leq z \leq h, \end{cases} \quad (32)$$

from which we obtain the following velocity and shear-stress profiles if we assume no slip at the bed:

$$u_x(z) = \begin{cases} \frac{g \sin \theta}{w_e} \left[ z - \frac{\nu}{w_e} \left( e^{-\frac{w_e}{\nu}(r-z)} - e^{-\frac{w_e}{\nu}r} \right) \right], & 0 \leq z \leq r; \\ \frac{g \sin \theta}{w_e} \left[ r - \frac{\nu}{w_e} \left( 1 - e^{-\frac{w_e}{\nu}r} \right) \right], & r \leq z \leq h, \end{cases} \quad (33)$$

$$\sigma_{xz}(z) = \begin{cases} \tau_y + \frac{\rho_f \nu g \sin \theta}{w_e} \left( 1 - e^{-\frac{w_e}{\nu}(r-z)} \right), & 0 \leq z \leq r; \\ \rho_f g (h - z) \sin \theta, & r \leq z \leq h. \end{cases} \quad (34)$$

By expanding the exponential functions to second order, one easily verifies that Eqs. (32)–(34) reduce to Eqs. (26)–(28) in the limit  $w_e \rightarrow 0$ .

An additional boundary condition must be imposed to determine an entrainment speed  $w_e$  that is compatible with the dynamical properties of the system. For many materials in which the shear stress is an increasing function of the shear

rate, there is a fundamental feedback mechanism: If the erosion rate is too small, the shear stress due to the downslope component of gravity is not completely balanced by the bed shear stress and the inertial forces due to the acceleration of eroded material, hence the flow velocity will increase. At the same time, the shear stresses also increase and lead to a higher erosion rate. Conversely, if the erosion rate is too large, the flow is decelerated so that the bed shear stress and thus the erosion rate diminish.

By combining microscopic and macroscopic considerations, the appropriate boundary condition may be determined: On average, a minimum shear stress (depending on the bed and flow materials) is needed to break a particle out of the bed surface,  $\sigma_{xz} \geq \tau_c$ . Right after a particle has broken loose, approximately the same force still acts on it and accelerates it. As soon as it has moved away a few particle diameters from its original location, the same average shear stress acts there again. If the time required to break the interparticle bonds is much shorter than the time required to move the particle out of the way, the erosion rate is limited by the entrainment process. Accordingly, the erosion rate attains the largest value that leaves the bed shear stress at its threshold value  $\tau_c$ . This is expected to be the case for materials that exhibit brittle behavior at the particle scale, among them snow or weakly cohesive sands under the action of strong flows. Only if the bed material is very ductile so that breaking it requires relatively long time and large deformations, will the supply of eroded particles be too low to diminish the bed shear stress to its minimum value. We conclude that for many if not most rapid gravity mass flows, the required boundary condition may be formulated approximately as

$$\sigma_{xz}(0) = \tau_c. \quad (35)$$

Note that very similar reasoning was used by Owen (1964) in the context of sand and snow drift. Inserting Eq. (34) into this condition, we obtain for the Bingham fluid

$$\frac{\rho_f \nu g \sin \theta}{w_e} \left( 1 - e^{-\frac{w_e r}{\nu}} \right) = \tau_c - \tau_y; \quad (36)$$

in the limit  $\tau_y \rightarrow 0$ ,  $r \rightarrow h$ , an eroding Newtonian fluid is recovered.

In order to compare the steady-state profiles of shear stresses, shear rates and velocities in Newtonian and Bingham fluids with and without entrainment, it is useful to scale the variables in the following way:

$$\zeta = z/h, \quad \psi = \sigma_{xz}/\sigma_0, \quad \psi_y = \tau_y/\sigma_0, \quad (37)$$

$$v = \frac{u_x}{\frac{g h^2 \sin \theta}{2\nu}}, \quad \varsigma = \frac{r}{h} = 1 - \psi_y, \quad \chi = \frac{w_e}{\nu/h},$$

where  $\sigma_0 = \rho_f g h \sin \theta$  will be called “gravitational traction” in the following. The expressions obtained after scaling are listed in Table 1, and Fig. 5 shows the scaled profiles for selected parameter values. In order to highlight the differences in the shapes of the velocity profiles, they are rescaled by the respective maximum velocity in Fig. 6.

**Table 1.** Vertical profiles of shear stress and longitudinal velocity in steady-state flows of Newtonian and Bingham fluids with and without entrainment. All quantities are non-dimensionalized according to Eq. (37). In the limit of vanishing entrainment, i. e.  $\chi \rightarrow 0$ , all profiles with entrainment reduce to the corresponding profiles without entrainment. The Boussinesq form factor  $f \equiv h \int_0^h u^2 dz / \left( \int_0^h u dz \right)^2$  is evaluated for  $\varsigma = 0.5$  for the Bingham fluid and for  $\psi = 0.7$  in the case of entrainment. The values of  $\chi$  indicated in brackets correspond to physically consistent entrainment rates.

	Interval	Shear-stress profile $\psi(\zeta)$	Velocity profile $v(\zeta)$	Boussinesq form factor $f$
Newtonian fluid, no entrainment	[0,1]	$1 - \zeta$	$2\zeta - \zeta^2$	1.2000
Newtonian fluid, entrainment	[0, 1]	$\frac{1}{\chi} \left( 1 - e^{-\chi(1-\zeta)} \right)$	$\frac{2}{\chi} \left[ \zeta - \frac{1}{\chi} \left( e^{-\chi(1-\zeta)} - e^{-\chi} \right) \right]$	1.2185 ( $\chi = 0.761434$ )
Bingham fluid, no entrainment	[0, $\varsigma$ ] [ $\varsigma$ , 1]	$1 - \zeta$	$2\zeta\varsigma - \zeta^2$ $\zeta^2$	1.1040
Bingham fluid, entrainment	[0, $\varsigma$ ] [ $\varsigma$ , 1]	$1 - \zeta + \frac{1}{\chi} \left( 1 - e^{-\chi(\varsigma-\zeta)} \right)$ $1 - \zeta$	$\frac{2}{\chi} \left[ \zeta - \frac{1}{\chi} \left( e^{-\chi(\varsigma-\zeta)} - e^{-\chi\varsigma} \right) \right]$ $\frac{2}{\chi} \left[ \zeta - \frac{1}{\chi} \left( 1 - e^{-\chi\varsigma} \right) \right]$	1.1095 ( $\chi = 4.462238$ )

**Table 2.** Examples of entrainment rates obtained for different combinations of snowcover strength ( $\tau_c$ ), yield strength ( $\tau_y$ ) and Bingham viscosity ( $\nu_B$ ) in the flow. Idealized stationary flow with constant density  $200 \text{ kg m}^{-3}$ , flow height 1 m and surface velocity  $20 \text{ m s}^{-1}$ .

$\tau_c$ [Pa]	$\tau_y$ [Pa]	$\nu_B$ [ $\text{m}^2 \text{ s}^{-1}$ ]	$w_e$ [ $\text{m s}^{-1}$ ]	$q$ [ $\text{kg m}^{-2} \text{ s}^{-1}$ ]
700	500	0.0168	0.075	15.0
800	600	0.0125	0.050	10.0
800	300	0.0489	0.050	10.0
900	600	0.0165	0.025	5.0

In depth-averaged models, the velocity profiles of non-entraining flows may also be used in the case of entrainment or deposition because the Boussinesq form factor (which appears in the momentum balance) changes only by a small amount as long as dynamically sustainable entrainment rates are specified, see the last column of Table 1.

Comparison of the predicted entrainment rates with experimental data is difficult because erosion rates have rarely been measured, and then mostly in dry-snow avalanches (Gauer and Issler, 2004; Sovilla, 2004) for which a Bingham fluid is a poor approximation. Nevertheless, assuming typical values such as a slope angle of  $30^\circ$ , a flow depth of 1 m, a density of  $200 \text{ kg m}^{-3}$  and a surface velocity of  $20 \text{ m s}^{-1}$ , we obtain the values listed in Table 2, which are of the right order of magnitude.

## 5 Differences between deposition and entrainment

At first sight, deposition might be thought of simply as entrainment with a negative erosion rate; a closer look, however, reveals subtle but important differences. In this section, we discuss the following three questions: (i) What are the necessary and sufficient conditions on the flow configuration and the material properties for deposition to occur? (ii) Can deposition cause the flowing mass to accelerate? (This question was raised by Hungr (1990) by noting the analogy of the model proposed by Cannon and Savage (1988) with the equations for rocket motion.) (iii) How does deposition affect the velocity profile of a flow?

Question (ii) arose from the observation that the equation of motion for a mass-changing object,  $d(mv)/dt = F$ , can be written as

$$m \frac{dv}{dt} = F_g - F_f - \frac{dm}{dt} v \quad (38)$$

in our case, with  $F_g$  the component of the gravitational force along the path,  $F_b$  the bed friction and  $v$  the velocity<sup>6</sup>. The flow accelerates if  $v dm/dt < F_g - F_b$  or, equivalently,  $v q_b < \sigma_0 - \sigma_{xz}^{(b)}$ , with  $q_b$  the bed entrainment rate (taking negative values for deposition); recall that  $\sigma_0 \equiv \bar{\rho} g h \sin \theta$ . The confusion in the cited works (and in the research community at large, as many discussions have shown) appears

<sup>6</sup>Equation (23) reduces to Eq. (38) if we integrate over the flow length and assume  $u_x^{(b+)} = u_x^{(s-)} = 0$ ,  $\partial_x b = 0$ , assuming a uniform velocity profile with  $\overline{u_x^2} = \bar{u}^2$ . The rocket equation is obtained from (38) by replacing the flow velocity on the right-hand side by the exhaust speed relative to the rocket. In the case of a GMF, friction at the bed causes the mass lost by the flow to be stopped, so the ‘‘exhaust’’ speed is equal to the flow velocity.

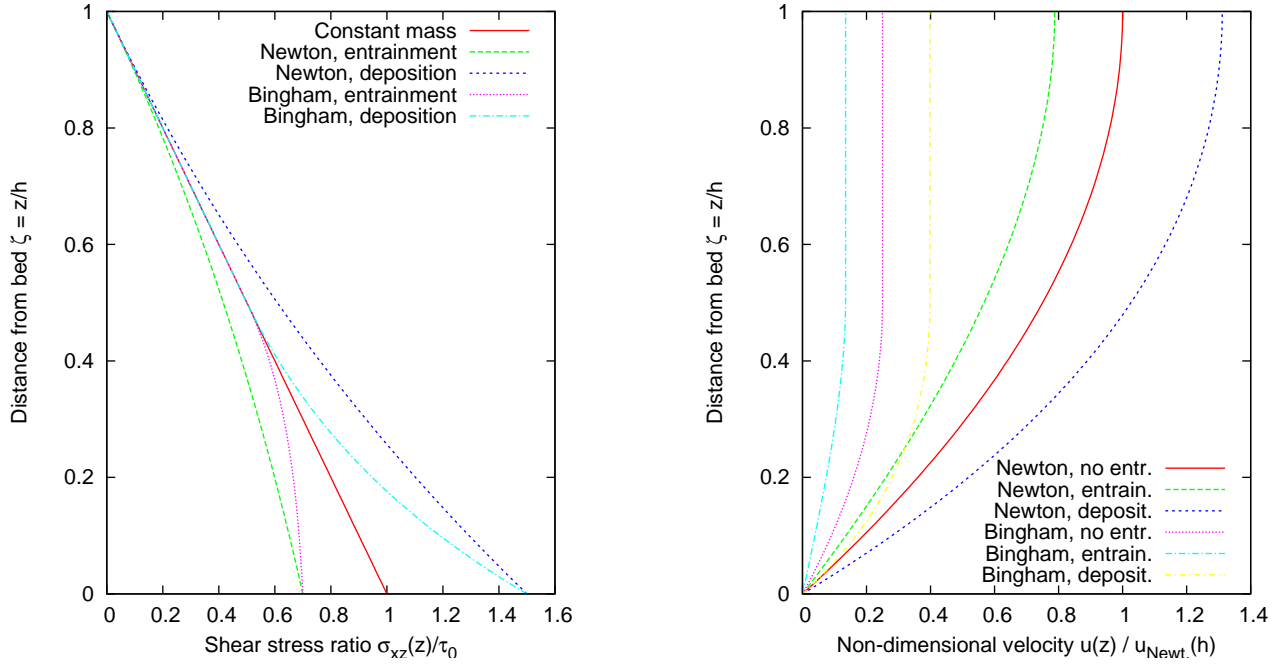


**Fig. 5.** Non-dimensionalized shear-stress (left) and velocity (right) profiles for stationary flows of Newtonian and Bingham fluids on an inclined plane, with and without entrainment or deposition. The parameter values are  $\zeta = 0.5$  for the Bingham fluid,  $\psi_c = \tau_c/\sigma_0 = 0.7$  for the entraining flows, and  $\sigma_{xz}(0)/\sigma_0 = 1.5$  for the depositing flows.

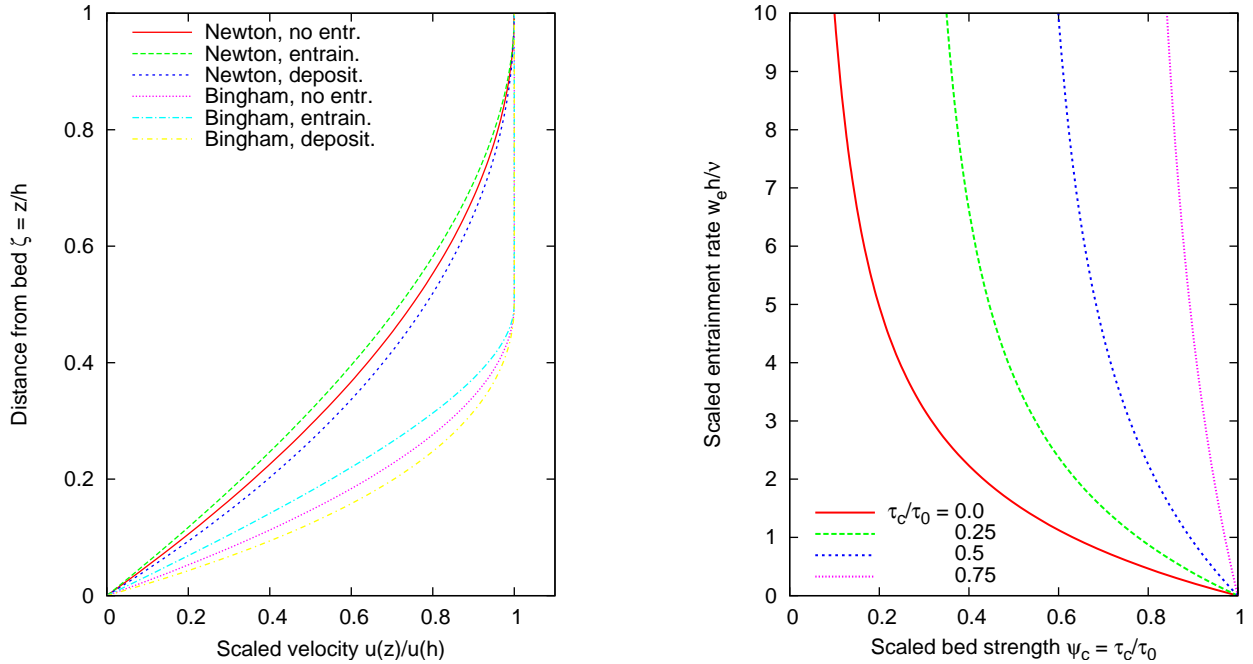


**Fig. 6.** Comparison of the shapes of the velocity profiles for non-entraining, entraining and depositing Newtonian and Bingham fluids, using the same parameter values as in Fig. 5. All profiles are scaled with their surface velocity so that  $v(1) = 1$ .

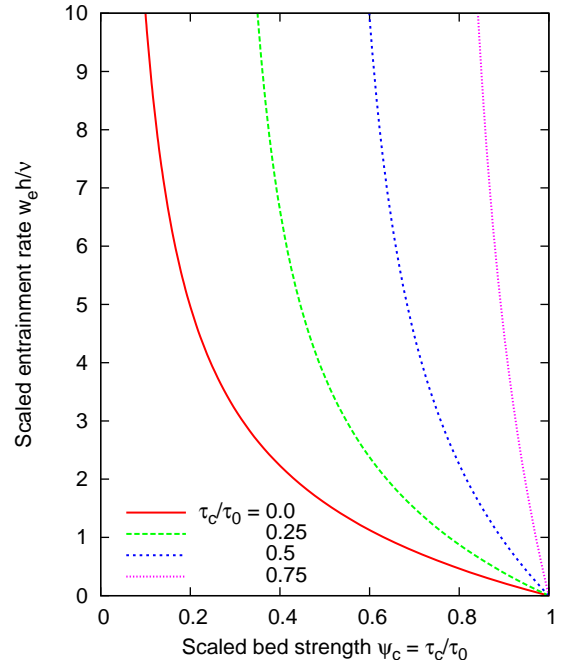


**Fig. 7.** Dependence of the entrainment rate on the bed shear strength  $\tau_c$  for various values of the yield strength  $\tau_y$  of the Bingham fluid. All quantities are non-dimensionalized according to Eq. (37).

to be caused by the fact that the acceleration of the rocket is due to internal forces within the system rocket–exhaust gases whereas the deposited mass in a GMF is brought to rest by (external) friction forces. Thus Erlichson (1991) supports Hungr’s view that the equation of motion (38) used by Cannon and Savage (1988, 1990) is faulty.

In order to demonstrate as intuitively as possible why Eqs. (38) and (23) are indeed correct but lack a constraint, we idealize the GMF as two sliding plug layers, namely a flowing layer on top with mass  $m$  per unit area and velocity  $v_f$  (assumed uniform with depth for simplicity), and a thin depositing layer underneath with mass  $\Delta m$  per unit area and velocity  $v_d$ . The thickness of the latter is chosen such that it comes to rest within the time interval  $\Delta t$ , from its initial value equal to  $v_f$ . Each layer is subjected to gravity and the depositing layer additionally to the bed shear stress  $\sigma_{xz}^{(b)}$ . The shear stress at the interface between the layers is designated by  $\sigma_{xz}^{(i)}$ . Then we get the following equations for the two layers:

$$m\Delta v_f/\Delta t = mg \sin \theta - \sigma_{xz}^{(i)}, \quad (39)$$

$$\Delta m \Delta v_d/\Delta t = \Delta mg \sin \theta + \sigma_{xz}^{(i)} - \sigma_{xz}^{(b)}. \quad (40)$$

According to the assumptions,  $\Delta v_d = -v_f$  and  $\frac{\Delta m}{\Delta t} = -q_b$ . Letting  $\Delta t \rightarrow 0$ , we obtain  $m\dot{v}_f = mg \sin \theta - \sigma_{xz}^{(i)}$  and  $q_b v_f = \sigma_{xz}^{(i)} - \sigma_{xz}^{(b)}$ , i. e., the motion of the flowing layer is determined by the shear stress transmitted inside the material whereas the deposition rate is governed by the difference between the bed shear stress and the internal shear stress near the bed. When we add the two equations, Eq. (38) results. Thus, in contradiction to Hungr’s and Erlichson’s opinion, the equation used by Cannon and Savage is correct also for deposition; no daemons actively shedding mass from the GMF are required, but the bed must exert a larger shear stress on the bottom flow layer than can be transmitted in the flowing material itself. If the main flow were to accelerate at all during deposition, this would not be due to the mass loss but to the intrinsic weakness of the flowing material.

The condition  $\sigma_{xz}^{(b)} > \sigma_{xz}^{(i)} > 0$  during deposition implies an upper limit on the deposition rate  $q_d$ :

$$q_d \equiv \max(0, -q_b) < \sigma_{xz}^{(b)}/v_f. \quad (41)$$

This is a loose upper bound, however, because in realistic situations we expect  $\sigma_{xz}^{(i)}$  to be close to  $\sigma_{xz}^{(b)}$ . Designating the force inside the flow due to shear by  $F_i$ , this constraint allows to write Eq. (38) as

$$m \frac{dv}{dt} = F_g - F_i < F_g, \quad (42)$$

making it evident that mass loss does not lead to unphysical acceleration.

We may now ask about necessary and sufficient conditions for sustained deposition to occur. If the material is homogeneous, i. e., not a suspension of particles in a fluid, we conclude from the preceding discussion that  $\sigma_{xz}^{(b)}$  must be larger

than  $\tau_{\max}^{(i)}$ , the maximum transmittable shear stress inside the GMF, which depends on the material properties. Moreover, the shear stress inside the material must be close to the gravitational traction. Under this condition, the bottom layer will decelerate while the main flow layer continues at high speed. This is not a sufficient condition, however: Once stopped, the originally flowing material must rapidly bond to the bed material and thereby inherit the frictional properties of the latter for  $\sigma_{xz}^{(b)}$  to remain larger than  $\sigma_{xz}^{(i)}$ .

Particle suspensions or granular materials with the capability for sintering may fulfill these conditions more easily: Particles that touch the bed at moderate speed (so that they do not eject other particles at impact) may be trapped in hollows formed by other particles. If the fluid shear stress or particle impacts are insufficient to dislodge them, bonds to the bed particles will develop. Furthermore, it is well known that granular materials usually have a static friction angle that is larger than the dynamic one, which means that they may fulfill the condition  $\sigma_{xz}^{(i)} < \sigma_{xz}^{(b)}$  as well.

Considering the intricacies of the deposition process, we conjecture that in many cases deposits found in the path of GMFs represent the stopped tail of the flow rather than material from the bottom of the main body. For example, high-speed video recordings of subaerial and subaqueous laboratory mudflows show how the tail of the flow is immobilized when the flow depth falls below a limiting value that is related to the yield strength of the slurry. All types of models except the mass-point ones can describe this flow behavior adequately without invoking any deposition model. In contrast, gradual settling-out of particles (often accompanied by normal grading of the deposits) has been directly observed in powder-snow avalanches, turbidity currents and sandy debris flows.

We may extend the preceding considerations to other flow conditions and characterize the behavior of a GMF in terms of the values of the bed shear stress,  $\sigma_{xz}^{(b)}$ , the shear strength or erosion threshold of the bed,  $\tau_c$ , and the gravitational traction,  $\sigma_0$ . Table 3 summarizes the possible relations between the stresses and the associated behavior of the flow. We assume that the longitudinal stress gradient is negligible. Even though we specify only the bed shear stress rather than the full stress profile, most flow situations arising in Nature can be sufficiently characterized in this way, except perhaps transient phases at abrupt changes of the slope angle or during rapid channeling, where the shape of the velocity profile changes quickly and significantly.

Table 3 suggests that steady-state flow over an erodible bed with neither entrainment nor deposition can occur if (i) the gravitational traction is below the bed erosion threshold,  $\sigma_0 < \tau_c$ , and (ii) there exists a velocity at which  $\sigma_{xz}^{(b)} = \sigma_0$ . This situation appears to be relevant to many gravity mass flows. It represents the limiting case between cases 4 and 5. Cases 3 and 4 represent transient situations that depend on the asymmetry between static and dynamic material proper-

**Table 3.** Characterization of flow situations (acceleration/deceleration, entrainment/deposition) in gravity mass flows in terms of the relation between the bed shear strength, the gravitational traction and the dynamically generated bed shear stress.

Case	Shear stress	Flow behavior
1	$\tau_c < \sigma_{xz}^{(b)} < \sigma_0$	The entrainment rate grows, driving $\sigma_{xz}^{(b)}$ towards its equilibrium value $\tau_c$ . Depending on the excess gravitational traction, the flow may be accelerating (e. g. after an abrupt steepening of the slope) or decelerating (after abrupt flattening of the slope with simultaneous reduction of $\tau_c$ ).
2	$\tau_c < \sigma_0 < \sigma_{xz}^{(b)}$	The entrainment rate is much too high, deceleration occurs to restore the balance and return to case 1. Typical situation after abrupt decrease of the slope angle to a value that, however, still allows entrainment in dynamical equilibrium.
3	$\sigma_{xz}^{(b)} < \tau_c < \sigma_0$	The bed shear stress is insufficient for entrainment and smaller than the gravitational traction, the flow accelerates and will eventually entrain as $\sigma_{xz}^{(b)}$ tends towards $\tau_c$ .
4	$\sigma_{xz}^{(b)} < \sigma_0 < \tau_c$	As gravitational traction is larger than the bed shear stress, the flow accelerates but will not be able to entrain bed material. It tends towards the equilibrium state $\sigma_{xz}^{(b)} = \sigma_0$ .
5	$\sigma_0 < \sigma_{xz}^{(b)} < \tau_c$	The flow decelerates. Deposition occurs under suitable circumstances.
6	$\sigma_0 < \tau_c < \sigma_{xz}^{(b)}$	The flow entrains even though it decelerates because the friction between the bed and the flowing material is larger than the bed strength. It tends towards case 5.

ties; deposition should not occur because the friction exerted by the bed is lower than the driving gravitational force.

To conclude this section and illustrate the similarities and differences between deposition and entrainment, we consider again the artificial steady-state flow system described in Sect. 4. In the case of deposition, material is supplied at the top at surface velocity and removed at the bottom after it has come to rest. Deposition makes the non-dimensionalized shear stress profile (cf. Fig. 5) convex instead of concave in the shear layer; the value at the bed interface exceeds the gravitational traction. Similarly, the velocity normalized by its value at the surface is larger in the shear layer than in the flow without deposition, opposite to the effect of entrainment (see Fig. 6). In contrast to the eroding flow, the material properties do not impose a boundary condition for the bottom shear stress in the depositing flow. The rate at which mass is supplied to the flow at its surface speed determines the flow velocity according to Eq. (33), with negative  $w_d$  instead of positive  $w_e$ . We stress, however, that determination of the deposition rate in more realistic situations requires explicit modelling of the flow dynamics and consolidation processes at the bed–flow interface, which cannot be carried out strictly within the framework of depth-averaged equations.

## 6 Conclusions

The main results of this investigation may be summarized as follows:

1. The correct formulation of the momentum balance in a flow with entrainment of ambient fluid or bed material requires careful definition of the system bound-

aries. Depending on those, different formulations may be obtained that need to be interpreted consistently. In the case of bed entrainment not due to isolated impacts, the most natural system definition leaves no “entrainment force” term in the momentum balance equation, but there is a significant retarding term  $-q\bar{u}$  in the equation of motion. Entrainment from moving ambient fluid or due to impact of isolated particles requires a momentum source term  $q\mathbf{u}|_{\text{interface}}$  in the momentum balance and a corresponding term in the equation of motion.

2. The velocity and shear stress profiles of entraining/depositing flows differ from those of non-entraining/non-depositing, but otherwise equivalent flows because of the gradual acceleration/deceleration of the entrained/deposited mass. The difference may be neglected in most practical applications, however. In the case of entrainment of brittle bed material, we gave arguments that the erosion rate tends to the value that makes the interfacial shear stress equal to the erosion threshold (if the flow is nearly stationary). Deposition depends on additional material properties that control the consolidation of the material, which are not well understood for most granular materials.
3. A practically important class of eroding flows are those limited by their entrainment capacity rather than by their erosive capacity. Our analysis in Sect. 4 showed how to determine the entrainment rate in the case of a particular entrainment-limited flow. This approach, based on the non-averaged balance equations, generally works in entrainment-limited situations, but closed-form solutions may be hard to find or may not exist.

4. When no closed-form solution is available, heuristic parameterizations have to be used, but they may be inconsistent with the internal dynamics of the flow. Only a more complete, non-averaged analysis will produce a fully consistent solution.

For a class of simple materials characterizable by an erosion threshold stress  $\tau_c$ , the entrainment behavior is thus essentially determined by the boundary condition for the stress at the bed–flow interface. Several flows of geophysical importance—among them snow and rock avalanches, perhaps also debris flows—may be adequately described in this way. However, the following general issues need to be considered in more detail: (i) How can the deviations of the velocity profile from its non-entrainment equilibrium shape be parameterized in a simple way applicable in one- and two-dimensional depth-averaged flow models? (ii) How rapidly do the velocity and shear-stress profiles adapt themselves to changed conditions, e. g. at slope breaks or due to variability of the bed material? (iii) How well can the erosion behavior of specific bed materials be described by a single threshold shear stress? (iv) How does the threshold shear stress depend on other, more easily measurable parameters of a given material?

The first question can be studied by searching for analytic solutions to simplified flow situations as the one assumed in Sect. 4. Of particular interest are expressions for rheologies other than Bingham and for situations where the flow depth is allowed to grow in proportion with the entrained mass and the velocity increases accordingly. In contrast, a numerical approach resolving the vertical dimension is probably needed to obtain answers to the second question, and it remains to be seen how to parameterize them for use in depth-averaged models.

The third question clearly requires dedicated experimental work, mainly in the laboratory along the lines indicated by Barbolini et al. (2005). If lateral high-speed video recordings can be obtained over the entire depth of the bed and the flow and over a sufficiently long distance in the flow direction, particle tracking allows evaluation of the acceleration  $d\mathbf{u}(x, z, t)/dt$  from  $\partial_t \mathbf{u}(x, z, t)$  and  $\nabla \mathbf{u}(x, z, t)$  in addition to the density and velocity profiles and the erosion rate. From these data, the shear stress profile can be estimated and Eq. (35) tested if  $\partial_x \sigma_{xx}$  may be neglected; also deviations from hydrostatic distribution of  $\sigma_{zz}$  can be quantified. While such measurements appear feasible, care must be taken to obtain sufficiently precise and reproducible results (for example, the shear strength of the bed material may vary significantly with humidity and temperature); also, direct verification of the condition  $\partial_x \sigma_{xx} \ll \partial_z \sigma_{zz}$  may be very difficult. The fourth problem will also require experimental work, the methods of which will have to be adapted to the specific properties of the material to be studied.

*Acknowledgements.* This work was funded by the EU 5th Framework Programme through the project SATSIE (EU Contract no.

EVG1–CT2002–00059) and by the Swiss National Science Foundation (grant no. 200021–101911). We are grateful to Massimiliano Barbolini, Margarita E. Eglit, Peter Gauer, Carl B. Harbitz and Mohamed Naaim for fruitful and enjoyable discussions that encouraged us to write this paper.

## References

- Barbolini, M., Biancardi, A., Cappabianca, F., Natale, L., and Pagliardi, M.: Experimental study of erosion processes in snow avalanches, *Cold Regions Sci. Technol.*, 43, 1–9; doi:10.1016/j.coldregions.2005.01.007, 2005.
- Briukhanov, A. V., Grigorian, S. S., Miagkov, S. M., Plam, M. Y., Shurova, I. Y., Eglit, M. E., and Yakimov, Y. L.: On some new approaches to the dynamics of snow avalanches, in: *Physics of Snow and Ice*, Proc. Intl. Conf. Low Temperature Science, Sapporo, Japan, 1966. Vol. I, Part 2, edited by Ôura, H., pp. 1223–1241, Institute of Low Temperature Science, Hokkaido University, Sapporo, Hokkaido, Japan, 1967.
- Cannon, S. H. and Savage, W. Z.: A mass-change model for the estimation of debris-flow runout, *J. Geol.*, 96, 221–227, 1988.
- Cannon, S. H. and Savage, W. Z.: A mass-change model for the estimation of debris-flow runout: A reply, *J. Geol.*, 98, 792, 1990.
- Eglit, E. M.: Some mathematical models of snow avalanches, in: *Advances in the Mechanics and the Flow of Granular Materials*, edited by Shahinpoor, M., vol. II, pp. 577–588, Trans Tech Publications, Clausthal-Zellerfeld, Germany, 1st edn., 1983.
- Eglit, M. E.: Mathematical and physical modelling of powder-snow avalanches in Russia, *Annals Glaciol.*, 26, 281–284, 1998.
- Eglit, M. E. and Demidov, K. S.: Mathematical modeling of snow entrainment in avalanche motion, *Cold Regions Sci. Technol.*, 43, 10–23; doi:10.1016/j.coldregions.2005.03.005, 2005.
- Erlichson, H.: A mass-change model for the estimation of debris-flow runout, a second discussion: Conditions for the application of the rocket equation, *J. Geol.*, 99, 633–634, 1991.
- Fukushima, Y. and Parker, G.: Numerical simulation of powder-snow avalanches, *J. Glaciol.*, 36, 229–237, 1990.
- Gauer, P.: Numerical modeling of blowing and drifting snow in Alpine terrain, *J. Glaciol.*, 47, 97–110, 2001.
- Gauer, P. and Issler, D.: Possible erosion mechanisms in snow avalanches, *Annals Glaciol.*, 38, 384–392, 2004.
- Gray, J. M. N. T., Wieland, M., and Hutter, K.: Gravity-driven free surface flow of granular avalanches over complex basal topography, *Proc. R. Soc. Lond. A*, 455, 1841–1874, 1999.
- Grigorian, S. S. and Ostroumov, A. V.: The mathematical model for slope processes of avalanche type (in Russian), Scientific Report 1955, Institute for Mechanics, Moscow State University, Moscow, Russia, 1977.
- Hermann, F., Issler, D., and Keller, S.: Towards a numerical model of powder snow avalanches, in: *Proc. of the Second European Computational Fluid Dynamics Conference*, Stuttgart (Germany), September 5–8, 1994, edited by Wagner, S., Hirschel, E. H., Périaux, J., and Piva, R., pp. 948–955, J. Wiley & Sons, Ltd., Chichester, UK, 1994.
- Hungr, O.: A mass-change model for the estimation of debris-flow runout: A discussion, *J. Geol.*, 98, 791, 1990.
- Issler, D.: Modelling of snow entrainment and deposition in powder-snow avalanches, *Annals Glaciol.*, 26, 253–258, 1998.

- Issler, D., Gauer, P., Schaer, M., and Keller, S.: Staublawineneignisse im Winter 1995: Seewis (GR), Adelboden (BE) und Col du Pillon (VD), Internal Report 694, Eidg. Institut für Schnee- und Lawinenforschung, CH-7260 Weissfluhjoch/Davos, Switzerland, 1996.
- Issler, D., Gauer, P., and Barbolini, M.: Continuum models of particle entrainment and deposition in snow drift and avalanche dynamics, in: *Models of Continuum Mechanics in Analysis and Engineering*, Proceedings of a conference held at the Technische-Universität Darmstadt, September 30 to October 2, 1998, edited by Baean, R., pp. 58–80, Shaker Verlag, Aachen – Maastricht, 2000.
- Naaim, M. and Gurer, I.: Two-phase numerical model of powder avalanche—theory and application, *Natural Hazards*, 117, 129–145, 1998.
- Naaim, M., Naaim-Bouvet, F., Faug, T., and Bouchet, A.: Dense snow avalanche modeling: flow, erosion, deposition and obstacle effects, *Cold Regions Sci. Technol.*, 39, 193–204, 2004.
- Owen, P. R.: Saltation of uniform grains in air, *J. Fluid Mech.*, 20, 225–242, 1964.
- Parker, G., Fukushima, Y., and Pantin, H. M.: Self-accelerating turbidity currents, *J. Fluid Mech.*, 171, 145–181, 1986.
- Rice, M. A., Willets, B. B., and McEwan, I. K.: Observations of collisions of saltating grains with a granular bed from high-speed cine-film, *Sedimentol.*, 43, 21–31, 1996.
- Sailer, R., Rammer, L., and Sampl, P.: Recalculation of an artificially released avalanche with SAMOS and validation with measurements from a pulsed Doppler radar, *Natural Hazards Earth Systems Sci.*, 2, 211–216, 2002.
- Savage, S. B. and Hutter, K.: The dynamics of avalanches of granular material from initiation to runout. Part I: Analysis, *Acta Mechanica*, 86, 201–223, 1991.
- Sovilla, B.: Field experiments and numerical modelling of mass entrainment and deposition processes in snow avalanches, Ph.D. thesis, Swiss Federal Institute of Technology, CH-8092 Zürich, Switzerland, 2004.
- Sovilla, B. and Bartelt, P.: Observations and modelling of snow avalanche entrainment, *Natural Hazards Earth Systems Sci.*, 2, 169–179, 2002.
- Sovilla, B., Somavilla, F., and Tomaselli, A.: Measurements of mass balance in dense snow avalanche events, *Annals Glaciol.*, 32, 230–236, 2001.
- Spring, U. and Hutter, K.: Numerical studies of jökulhlaups, *Cold Regions Sci. Technol.*, 4, 227–244, 1981.
- Takeuchi, M.: Vertical profile and horizontal increase of drift-snow transport, *J. Glaciol.*, 26, 481–492, 1980.
- White, B. R.: Two-phase measurements of saltating turbulent boundary layer flow, *Intl. J. Multiphase Flow*, 8, 459–473, 1982.